Dual Model Predictive Controlled Hybrid Energy Storage System for Naval DC Microgrids

Zheng, Zixuan; Chen, Xulin; Hu, Wenxi; Wang, Ying; Zong, Yi; Huang, Chunjun; Ni, Fuyao

Published in:
IEEE Transactions on Transportation Electrification

Link to article, DOI:
10.1109/TTE.2022.3177296

Publication date:
2023

Document Version
Peer reviewed version

This article has been accepted for publication in a future issue of this journal, but has not been fully edited. Content may change prior to final publication. Citation information: DOI 10.1109/TTE.2022.3177296, IEEE Transactions on Transportation Electrification

Dual Model Predictive Controlled Hybrid Energy Storage System for Naval DC Microgrids

Zixuan Zheng, *Member, IEEE*, Xulin Chen, Wenxi Hu*, Ying Wang, *Senior Member, IEEE*, Yi Zong, *Member, IEEE*, Chunjun Huang, Fuyao Ni

***Abstract*—Hybrid energy storage system (HESS) is an effective measure to improve the electrical performance of naval DC microgrids supplying power pulsed loads (PPLs). Coordination control scheme and capacity configuration of the HESS are two key issues to meet multiple control objectives and constraints. In response to the requirements of optimal operation for HESS under various complex scenarios, a dual model predictive control (D-MPC) strategy is proposed for the HESS integrated with the superconducting magnetic energy storage (SMES) and battery in this paper. Firstly, the current reference of battery is obtained through the MPC integrated adaptive low-pass filtering (ALPF). Then the local MPC controller of HESS converter is utilized to track the current reference of battery and SMES as well as the bus voltage reference to achieve transient power allocation of HESS and energy balancing of DC microgrid. Meanwhile, a cost function with adaptive weighting factor is designed to make tradeoff of conflict control objectives. Furthermore, the HESS capacity configuration and superconducting magnet optimal design according to its actual operation condition are presented. Comparative case studies are conducted in HIL experiment to demonstrate the superiority of the proposed scheme in terms of improving system operation performance under various PPLs.**

***Index Terms*- naval DC microgrid, pulsed power loads (PPLs), hybrid energy storage system, model predictive control (MPC), control of DC-DC converters.**

I. INTRODUCTION

NAVAL DC microgrids with advantages of high efficiency, reliability, and controllability have attracted wide attention recently [1]-[4]. Compared with terrestrial systems, the step change in load on shipboard system accounts for a higher percentage of available stored energy, and the system voltage stability is more susceptible. The shipboard loads consist of pulsed power loads (PPLs), propulsion, ship service, and dedicated high-power load, among which the PPL can be categorized into two types: pulsed loads such as laser weapons and the changing modes of operation of dedicated high-power load [2]. Diesel generation system as the main power supplier of shipboard has the relatively slow dynamic response to repeated large amount of PPL, causing a challenge to the power quality of the systems, including the voltage drop and swell even collapse of the power supplying system [5]. Moreover, the increasing power of electronic devices on shipboard are sensitive to power quality problems [6]. The traditional strategy meets the various load demands by increasing the system configuration capacity leading to relatively high volume and weight requirements of the ship's power equipment [7], which is at the expense of system efficiency and cost.

Integration of hybrid energy storage system (HESS) can improve the power quality of the naval DC microgrids as well as the operational and economic efficiency of the system [8]-[9]. The power-type energy storage devices such as supercapacitor, flywheel, and superconducting magnetic energy storage (SMES) have the advantages of fast responses high power density, long life cycle, long lifetime, and high conversion efficiency [10], which can effectively support the ON/OFF operation of pulse loads. The HESS scheme is achieved by combining power-type energy storage devices with the battery which has high energy density, high power capital cost, and slow response. By optimizing the coordinated control scheme and proper design of HESS, the operating characteristics of PPLs can be further improved on maintaining the safe and stable operation of the system. Different from supercapacitors, SMES is the inductive energy storage system of which control is relatively simple and without the need of step-up or step-down converters [11]. Moreover, the SMES has higher efficiency and lifespan than supercapacitor[10].

The HESS should meet the multiple and variable requirements in naval DC microgrids due to the complex working conditions. Since the energy storage systems (ESSs) are connected to the DC bus of naval microgrid through the converters, a robust, fast, and efficient control scheme of converters plays an important role in balancing dynamic power. A proportional-integral (PI) regulator and droop control-based controller for converters of HESS coordinated with diesel generator sets were proposed in [7]. This method calculated

Zixuan Zheng, Xulin Chen, Wenxi Hu, Ying Wang are with the College of Electrical Engineering, Sichuan University, China (e-mail: scuzzx@163.com; chenxulin000@163.com; 408803186@qq.com; tuantuan1125@scu.edu.cn;).

Yi Zong, Chunjun Huang are with the Department of Wind and Energy Systems, Technical University of Denmark, Denmark (e-mail: yizo@elektro.dtu.dk; chunhua@elektro.dtu.dk).

Fuyao Ni is with the Chengdu Electric Power Company, State Grid Sichuan Electric Power Company, China (e-mail: 603590155@qq.com).

the required average power for the diesel generator sets to improve the fuel consumption efficiency. The PI control with cascaded structure and saturation effect causes the sluggish response [19]. In addition, as a linear controller, the parameters tuning of PI control is frequently necessary and complex due to the nonlinear power converters and variability of load demands. Alternatively, model predictive control (MPC) provides a powerful framework to control power converters with constraints and handle multi-variable and objective cases [12]-[20]. Ref [15],[18] proposed the moving discretized control set (MDCS)-MPC for dual-active-bridge converters in naval DC microgrid, which provided low computational burden and stiff DC bus voltage regulation. In addition to voltage regulation, the automatic energy recovery of the power type energy storage system in HESS is significant for safe operation of both HESS and naval DC microgrid. However, the energy recovery of power-type energy storage and DC bus voltage control are conflicted control objectives, of which weighting factors need to be further studied [16]. In [8], the MPC controller has been designed for DC-DC converters for both supercapacitor and BESS which addressed the hard constraints of both input and output signals by combining MPC with linear matrix inequality. The transient power allocation in HESS is neglected due to the circuit designed specifically for supplying pulse loads. Different types of ESSs will handle the PPL demands separately without power allocation, thus affecting the lifespan and dynamic responses of HESS connected to the DC bus [17].

Currently, power allocation method decomposes the power demands into high and low-frequency components mainly by low-/high-pass filters [21]. Filtration method can realize the transient power allocation without communication. However, the cut-off frequency of filter is difficult to be accurately calculated, and which is typically determined through trial and error. In addition, the conventional fixed coefficient low-pass filtering has the problem of either the sub-high frequency signal not being filtered when the filter coefficient is too large or the large amplitude signal not being followed well when the filter coefficient is too small. Ref [22], [23] proposed the fuzzy logic control-based adaptive low-pass filtering method to take state of charge (SoC) of the ESSs into consideration, rectifying initial filter coefficient and keeping the SoC within a reasonable range, then prevent the instantaneous high current of the battery. Ref [24] proposed the dynamic filter coefficients based on identifying the charge and discharge modes of HESS to effectively reduce the charge/discharge cycles of BESS. Although the SoC of ESSs could be controlled within desired range by introducing the fuzzy logic control, the issue of constant filter coefficient in complex and varied operation conditions remains unsolved. Ref [25] proposed a fast MPC to achieve voltage control and power allocation in the HESS. However, the droop control introduces steady-state voltage deviation and the energy recovery of SMES is not considered. Furthermore, Ref [26] integrates the advantages of split-frequency methods and power-level methods, proposed an adaptive frequency-split-based quantitative power allocation strategy. In addition, to maximize the benefits of the HESS, SMES as power-type energy storage system is mainly used to compensate the initial and frequent power fluctuations before the start of the battery. Thus, as fast response controller that requires only local signal needs to be developed for taking full advantages of SMES.

Motivated by the above considerations, this paper proposes a dual model predictive control (D-MPC) method for controlling the HESS containing SMES and batteries in naval DC microgrid. The proposed method combines two MPC algorithms and applies a low-pass filter (LPF). The LPF based on MPC-I is used to generate the reference current of battery and assign the low-frequency component of the power demand to battery, while MPC-II incorporates the Model Predictive Voltage Control (MPVC) of the SMES and the Model Predictive Current Control (MPCC) of battery to drive the converter of the HESS. The main contributions of this paper are: (1) an adaptive filtering method combining model predictive control and low-pass filter is proposed; (2) an adaptive weighting factor is added to the cost function in MPC-II to achieve fast DC bus voltage regulation and automatic energy recovery of the SMES.

II. THE PROPOSED D-MPC CONTROL STRATEGY

A. Naval DC microgrid with HESS

DC naval microgrids are generally composed of diesel generator (DG) sets, SMES-battery HESS, and different types of loads. Fig. 1 shows the simplified diagram of a DC naval microgrid in single DC bus topology. The DG sets are the main supplier part of the naval DC microgrid, which provides average power under normal conditions. The DG sets supply for the AC bus of the shipboard system and is interfaced with DC bus by a voltage source converter (VSC). The propulsion loads are supplied by the AC bus and are not focused on in this paper. HESS operates as an energy buffer of the DC microgrid, which provides sufficient response to address possible load changes due to PPLs. The SMES is integrated to the DC bus through the DC/DC chopper. The batteries are interfaced with the DC bus by the double phase interleaved buck/boost converter which can reduce the impact of the large current of PPL on the power electronics switch as well as ripple coefficient of BESS.

Generally, the PPLs in naval DC microgrid group could be categorized into two types: pulsed loads (Type-A PPL) and change operation mode of radar load (Type-B PPL) as shown in Fig. 1. The Type-A PPL such as directed energy weapons in military ships draws a large amount of power from the system repeatedly, of which the duty cycle and the frequency are D_1 and T_1 respectively. The Type-B PPL such as certain military radar under changing modes of operation conditions, of which period and duty cycle of load power fluctuation is uncertain. The average load power varies greatly and the load power fluctuation rate is also variable as depicted.

To improve energy efficiency of diesel generation system [7], this paper assumes the constant power output during continuous PLL of the diesel generators, due to the relative slow dynamic response ability of diesel generators. Thus, the power insufficiency will appear in the DC microgrid as pulse ON and lead to voltage sag, while power surplus will appear as pulse OFF and lead to voltage swell. Thus, the HESS needs to discharge and charge as fast as possible when pulse ON and

This article has been accepted for publication in a future issue of this journal, but has not been fully edited. Content may change prior to final publication. Citation information: DOI 10.1109/TTE.2022.3177296, IEEE Transactions on Transportation Electrification

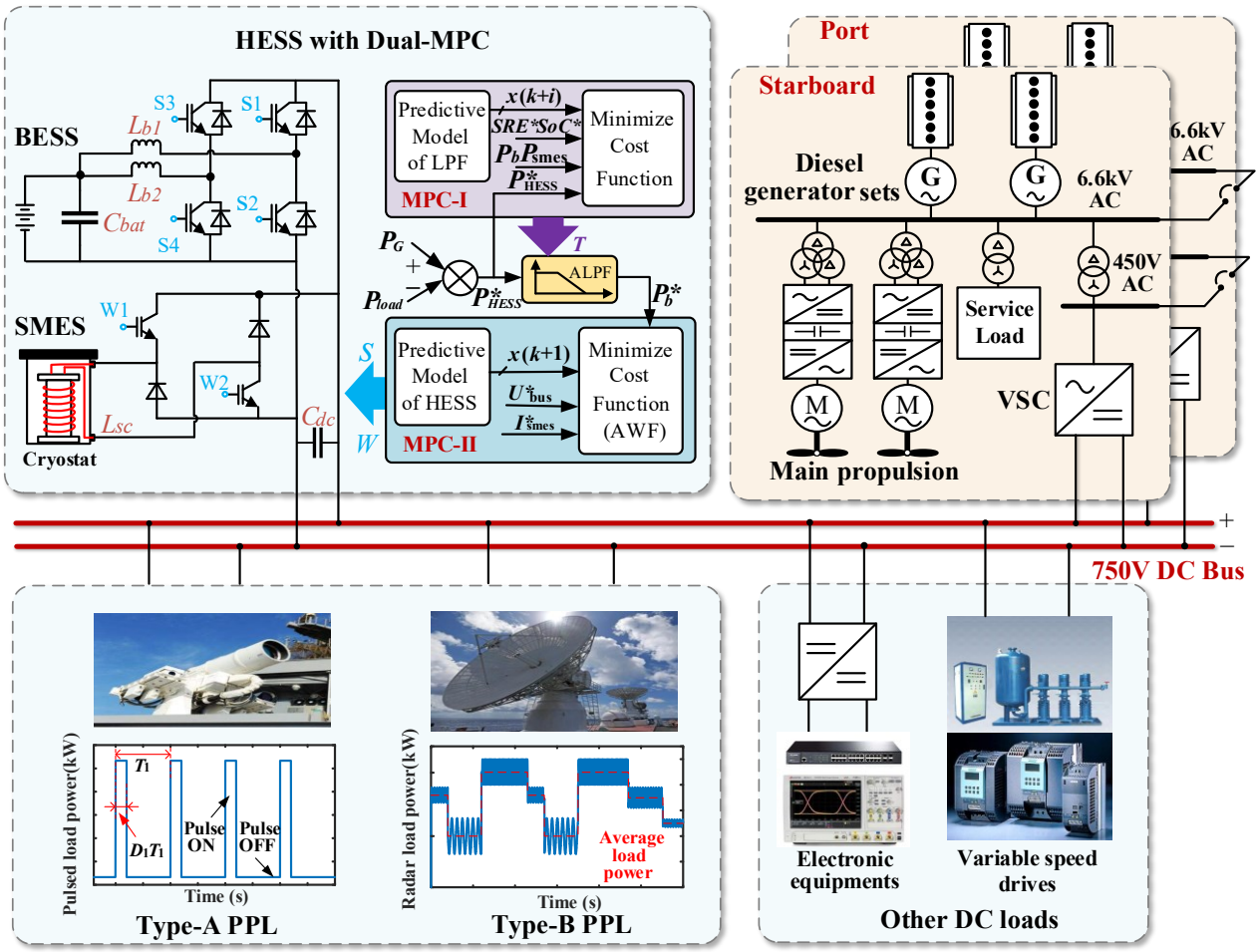

Fig. 1. The simplified diagram of naval DC microgrid with SMES-BESS HESS.

OFF respectively and maintains the stability of the DC bus. Furthermore, HESS control should take different characteristics of SMES and battery into consideration to optimize the energy utilization and sustainability. The multiple functions bestowed by the proposed strategy can be summarized as follows:

a) Dynamic DC bus voltage restorations: controlling HESS for fast dynamic power balancing, thus achieving DC bus voltage regulation and assistance in maintaining a stable output of DG sets.

b) Transient power allocation in HESS: the SMES supply the instantaneous high-power demands, while the batteries deal with the low-frequency parts. The batteries keep standby under high-frequency pulsed load if the residual energy of SMES is adequate. Therefore, reducing the dynamic response requirement of battery, which is of benefit to extending battery lifetime and enhancing the performance of naval DC microgrid.

c) Autonomous energy recovery of HESS: HESS consecutive discharging under load pulses may cause over-discharge problems and even cause HESS to quit operation. To recover the stored energy, controlling HESS to absorb the surplus power, thus maintaining a high level of energy for the coming PPL.

B. MPC-I

1) Low-pass filtering

The output of the ALPF in Fig.1 is the smoothed battery power demand P^*_b. The input of the ALPF is the reference power of HESS, which is power gap between the generation and consumption. The reference battery power $P^*_b(t)$ and reference HESS power $P^*_{HESS}(t)$ at time t can be obtained by the following equations:

$$\begin{cases} P^*_{HESS}(t) = P_G(t) - P_{Load}(t) \\ P^*_b(t) = (1-k(t)) \times P^*_b(t-1) + k(t) \times P^*_{HESS}(t) \end{cases} \quad (1)$$

where, $k(t)$ is the filter coefficient and $k(t)=T_s/T$, $k(t)$ is generally between 0 and 1. T_s is the sampling time and T is the time constant of LPF. For a control system, the sampling time is fixed, thus we can adjust the time constant T to change the filtering effect. The larger the time constant T, the smoother the filter results are. The smaller the time constant T, the higher sensitivity is.

2) MPC-I for adaptive filter time constant

The mathematical model of LPF is established for prediction at first. Then the cost function in the MPC-I defines the desired adaptive filter time constant. Considering that the proposed

MPC-based time constant adjusting method is executed in discrete-time domain and the sampling time is T_s. Due to the fast control of battery current tracking of MPC-II, the actual value of battery power can be regarded as equal to the reference value. The predictive model of LPF is given in (2) according to (1).

$$P_b(k+1) = P_b(k) + \frac{T_s}{T(k)}(P^*_{HESS}(k+1) - P_b(k)) \quad (2)$$

where $T(k)$ is the only manipulate variable of the MPC-I. $P_b(k)$ is the real-time charge or discharge power of battery at instant k, and $P_b(k+1)$ is the predictive charge or discharge power of battery at instant $k+1$.

The HESS power at instant $k+1$ is calculated as:

$$P_{HESS}(k+1) = P_b(k+1) + P_{SMES}(k+1) \quad (3)$$

where P_b $(k+1)$ and P_{SMES} $(k+1)$ are the battery and SMES predictive output power at instant $k+1$ respectively. When the sampling frequency is sufficiently high, P_{SMES}, DG output power $P_{G,}$ and load power P_{load} can be regarded as constants, and the discretization of P^*_{HESS} and P_{SMES} in (2) and (3) can be obtained as follows:

$$\begin{aligned} P^*_{HESS}(k+1) &= P_G(k+1) - P_{load}(k+1) \\ &= P_G(k) - P_{load}(k) = P^*_{HESS}(k) \end{aligned} \quad (4)$$

$$P_{SMES}(k+1) = P_{SMES}(k) \quad (5)$$

Therefore, (5) can be substituted into (3) to be a part of the prediction model of MPC-I.

Moreover, the state of residual energy (SRE) in SMES can be defined as:

$$SRE = \frac{E_{SMES}(t)}{E_{SMES\_ref}} = \frac{\frac{1}{2}L_{SC}i^2_{smes}}{\frac{1}{2}L_{SC}I^{*2}_{smes}} \times 100\% \quad (6)$$

where $E_{\mathrm{SMES\_ref}}$ and $E_{\mathrm{SMES}}(t)$ are the reference energy and real-time energy of SMES respectively, L_{SC} is the SMES inductance value, i_{smes} is the real-time SMES current and I^*_{smes} is the reference current of SMES. Suppose the BESS capacity is C_b, the state of charge (SoC) of BESS and the SRE of SMES can be calculated. In all, the prediction model of MPC-I is presented as:

$$\begin{cases} P_b(k+1) = P_b(k) + (T_s/T(k)) \times (P^*_{HESS}(k) - P_b(k)) \\ P_{HESS}(k+1) = P_b(k+1) + P_{SMES}(k) \\ SoC(k+1) = SoC(k) - T_s P_b(k)/C_b \\ SRE(k+1) = SRE(k) - T_s P_{SMES}(k)/E_{SMES\_ref} \end{cases} \quad (7)$$

There are two control objectives of MPC-I, one is reducing fluctuation of battery output power as well as the charge/discharge cycles of battery, the other is tracking HESS reference power for each control step. Thus, the cost function of MPC-I is given as:

$$J_1 = \min \sum_{i=k}^{k+m} \{[(P_b(i+1) - P_b(i)]^2 + [P_{HESS}(i+1) - P^*_{HESS}(i+1)]^2\} + \rho_{\varepsilon 1} \quad (8)$$

where m is the prediction horizon of MPC-I, which means the MPC-I controller must evaluate m future time steps when optimizing manipulated variable $T(k)$.

The relevant constraints consist of the minimum and maximum limit of the *SoC* of battery and the *SRE* of SMES as:

$$\begin{cases} k_{Pb\min 1} \times P_{b\_\min} < P_b(i) < k_{Pb\max 1} \times P_{b\_\max} \\ k_{SoC\min 1} \times SoC_{\min} < SoC(i) < k_{SoC\max 1} \times SoC_{\max} \\ k_{SRE\min 1} \times SRE_{\min 1} < SRE(i) < k_{SRE\max 1} \times SRE_{\max 1} \end{cases} \quad (9)$$

where the $k_{Pb\min 1}$, $k_{Pb\max 1}$, $k_{SoC\min 1}$, $k_{SoC\max 1}$, $k_{SRE\min 1,}$ and $k_{SRE\max 1}$ are coefficients that quantify the relaxation of the corresponding constraint. In order to take full consideration of remaining capacity of HESS, the hard constraints are selected in MPC-I algorithm, thus the $k_{x\min 1}$ (x=P_b, *SoC*, *SRE*) is greater than 1 and the $k_{x\max 1}$ (x=P_b, *SoC*, *SRE*) is less than 1. In this way, the hard constraints can ensure that the adaptive adjustment of the power distribution is realized before the SRE or SOC reaches the upper and lower limits. Over-charge and over-discharge problems with any one of the storage devices are avoided. Additionally, the weight $\rho_{\varepsilon 1}$ equals zero when the constraints are not violated and as an infinity value in cost function (8) penalizes the violation of the constraints.

C. MPC-II

1) Variables of the MPC-II

The control target of the converter's controller is to control the supplied and absorbed power of SMES and batteries to compensate the power gap caused by PPLs. Since the power supplied or absorbed by HESS is actually controlled by switching two of DC/DC converters, it is necessary to obtain the effect of switching states on the power supplied/absorbed [30].

The SMES charges when W1 and W2 are ON, discharges when W1 and W2 are off, and operates in storage mode without power exchange with the DC microgrid when W1 and W2 are opposite. Therefore, the signal of W1 is equal to W2 once the DC bus voltage deviation is larger than the threshold value by the enable signal of SMES. The two-phase interleaved buck/boost converter of BESS consists of two parallel buck/boost circuits, of which switches S1/S2 and S3/S4 could be opposite signals and the conduction time difference is $T_s/2$. Therefore, only two manipulated variables (S/W) for MPC-II are enough for generating all the output switching signals (W1/W2/S1/S2/S3/S4).

As shown in Fig. 1, except the battery reference power output from MPC-I, the input signals of MPC-II are measured in the HESS. The C_{dc} is the capacitance of the terminal of the HESS, L_{SC} is the inductor of superconducting magnet with L_{b1} and L_{b2} representing equivalent inductors of the converter in BESS. The i_{smes} is the real-time current of the SMES coil, i_b is output current of BESS, u_{bus} means the real-time bus voltage of the naval DC microgrid and i_{dc} is the current flows from the HESS to the microgrid. Firstly, the measurements and the parameters are taken into the predictive model to predict the output variables at instant $(k+1)$ based on the information available at instant k. Then the different combinations of switching states will be evaluated by comparing the predictive values and the reference values. Finally, the switch signals of minimum cost function are applied to the converters.

This article has been accepted for publication in a future issue of this journal, but has not been fully edited. Content may change prior to final publication. Citation information: DOI 10.1109/TTE.2022.3177296, IEEE Transactions on Transportation Electrification

2) Modeling of HESS

Fig. 2 shows the equivalent circuit of the SMES-battery HESS in the naval DC microgrid as operating in four different switching states. The parallel inductors of two-phase interleaved converter of BESS are equivalent to one phase inductance L_b, and the current through the two inductors is equivalent to i_b. This paper sets the current direction in power supplied mode as the positive direction. It can be observed the current and voltage relationship between energy storage systems and the DC bus.

According to the equivalent circuit and KVL, the dynamic models of the SMES and BESS current are presented in (10) and (11).

$$\begin{cases} L_{SC}\dfrac{di_{\text{smes}}}{dt}=u_{bus} & W=0 \\ L_{SC}\dfrac{di_{smes}}{dt}=-u_{bus} & W=1 \end{cases} \tag{10}$$

$$\begin{cases} L_b\dfrac{di_b}{dt}=u_{bat} & S=1 \\ L_b\dfrac{di_b}{dt}=u_{bat}-u_{bus} & S=0 \end{cases} \tag{11}$$

The equivalent capacitance of the HESS is modeled by the C_{dc} in Fig. 2, which can absorb and release power immediately. According to KCL, the change of bus voltage u_{bus} can be calculated based on the manipulated variables S and W as:

$$C_{dc}\frac{du_{bus}}{dt}=-i_{dc}+(1-W)\times i_{smes}+(1-S)\times i_b \tag{12}$$

Considering that the proposed MPC-based method is executed in discrete-time domain and the time step is T_s. (10), (11) and (12) need to be discretized using the forward Euler method, which is expressed as:

$$\begin{cases} i_{smes}(k+1)=\dfrac{T_s}{L_{SC}}\left[(1-W)u_{bus}(k)\right]+i_{smes}(k) \\ i_{bi}(k+1)=\dfrac{T_s}{L_{bi}}\left[u_{bat}(k)-Su_{bus}(k)\right]+i_{bi}(k),\ (i=1,2) \\ u_{bus}(k+1)=\dfrac{T_s}{C_{dc}}\left[(1-W)i_{smes}(k)+(1-S)i_b(k)-i_{dc}(k)\right]+u_{bus}(k) \end{cases} \tag{13}$$

In equation (13), $i_{smes}(k+1)$, $i_{bi}(k+1)$, and $u_{bus}(k+1)$ are the predictive values of the SMES current, BESS inductor current, and the DC bus voltage. Thus, the prediction model (13) can be used for the prediction of the possible future values for implementing the MPC-II algorithm.

3) Cost function of MPC-II

Under PPLs disturbances, the DC bus voltage is the main control objective of converter's controller. The control of SMES coil current should also be considered for maintaining enough energy of the SMES to deal with continuous load pulses. Additionally, the BESS can be controlled by minimizing the deviations of the inductor current from its reference value. Thus, the cost function which defines the desired behavior of HESS can express as (14).

In equation (14), u_{bus}^*, i_{smes}^* and i_{bi}^* are the reference values of DC bus voltage, SMES coil current, and BESS inductors current respectively. During the PPLs, the u_{bus}^* and i_{smes}^* could be the constant rated values, while the i_{bi}^* (i=1,2) is obtained by dividing reference battery power P_b^* by u_{bat}. Besides, considering that the control of SMES and battery current are the two main targets of MPC-II, the weighting factor of DC bus voltage term and the battery current term are both set to 1 in this article. And λ is the weighting factor that defines the tradeoff among the SMES coil current due the conflict of those two targets.

Furthermore, the weight $\rho_{\varepsilon 2}$ has an infinity value when the constraints are violated. The variables of constraints of MPC-II are the same as MPC-I. But at this time, the soft constraints are applied by choosing less than 1 value of $k_{x\min 2}$ and greater than 1 value of $k_{x\max 2}$ (x=P_b, SoC, SRE). The soft constraints have advantages of extending the operation range of HESS.

4) Adaptive weighting factor

Assume four pulses of 500 kW Type-A PPL occurs at t=1s as shown in Fig. 1, which has the frequency of 1Hz and the duty cycle of 20%. Fig. 3 illustrates the simulation results based on different weighting factor of λ. The response result for λ=1 is shown in Fig.3 (a), while Fig.3 (b) shows them for λ=0.01. It can be seen that an obvious DC bus voltage dropping is shown in Fig.3 (a) which can affect the normal operation of sensitive loads in naval system. In Fig. 3(b), the DC bus voltage is maintained in a small range, but SMES coil current drops significantly, and the BESS is switched in to charge and discharge. The increasing number of charge/discharge cycles of the BESS can result in lifetime attenuation. It can be concluded that a better DC bus voltage regulation performance is achieved with a low setting of λ, while the desired SMES capacity is ensured by setting higher value of λ. For this reason,

$$J_2=[u_{bus}(k+1)-u_{bus}^*]^2+\lambda[i_{smes}(k+1)-i_{smes}^*]^2+\sum_{i=1}^{2}[i_{bi}(k+1)-i_{bi}^*]^2+\rho_{\varepsilon 2} \tag{14}$$

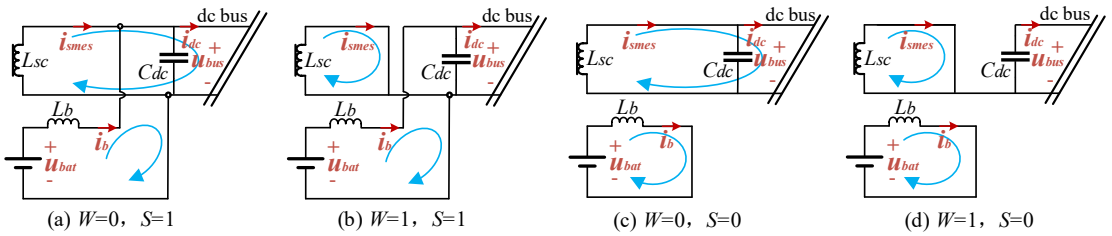

Fig. 2. Equivalent circuit of a HESS in the DC MG as operating in four different switching states.

This article has been accepted for publication in a future issue of this journal, but has not been fully edited. Content may change prior to final publication. Citation information: DOI 10.1109/TTE.2022.3177296, IEEE Transactions on Transportation Electrification

$$\lambda_a = \begin{cases} 0.01\times\exp[(i_{smes}-I^*_{smes})\times\dfrac{In(100)}{(I_{smes\_cri}-I^*_{smes})}] & ,(|\Delta U|>0.01p.u.\,\&\,i_{smes}>i^*_{smes}) \\ 0.01\times\exp[(I^*_{smes}-i_{smes})\times\dfrac{In(100)}{(I^*_{smes}-I_{smes\_min})}] & ,(|\Delta U|>0.01p.u.\,\&\,i_{smes}\le i^*_{smes}) \\ 1 & ,(|\Delta U|\le 0.01p.u.) \end{cases} \quad (15)$$

the adaptive weighting factor λ_a is proposed in (15) to capture the best features of these two variables. The curve of the adaptive weighting factor of the SMES current is shown in Fig. 3(c).

In equation (15), I_{smes_min} is the minimum limit of the SMES coil current and I_{smes_cri} the critical value of the SMES coil, I^*_{smes} is the predefined normal operation current of SMES inductance.

When absolute value of the voltage deviation (ΔU) is less than 0.01 p.u., the control objective of tracking the DC bus voltage is not that important and the SMES coil reference current tracking becomes the main target, thus set λ_a=1. When voltage deviation reaches 0.01 p.u., the DC bus voltage control turns into the main objective, where 0.01 is the value of λ as no SMES current error. In order to avoid quenching and over-discharge, the closer to the limit, the greater the λ_a according to (15) as shown in Fig. 3(c). The λ_a reaches the value of 1 when the SMES current reaches I_{smes_cri} or I_{smes_min}.

Then, Fig. 3(d) shows the value of adaptive weighting factor λa changes during four pulsed loads and Fig. 3(e) shows the effect of the proposed adaptive weighting factor: The DC bus voltage is quickly stabilized after every pulse ON, and maintained at a small range less than ±1% under pulsed loads. Meanwhile, the SMES current returned to the original reference value at every pulse OFF and kept operating in normal range.

D. Flow Diagram of Control Scheme

Flow diagram of the proposed D-MPC control scheme for HESS is shown in Fig. 4. Left-side and right-side flow block diagrams represent the process of the MPC-I and MPC-II respectively. The steps of MPC-I and MPC-II controller in each sampling period consist of: initialization, reading measurements, predicting future variables and minimizing cost function. For MPC-I, the prediction horizon is m, which means m steps future values of battery and HESS output power, as well as SoC and SRE, are predicted by the prediction model. In addition, the number of possible discrete-time constant T is n, thus the MPC-I executes the inner loop for n times to obtain the minimized cost function and the corresponding optimal time constant. For MPC-II, it is based on a single-step FCS-MPC, the prediction horizon is 1 and the number of possible switching signal combinations is 4, which has the advantages of small computational burden and fast response speed. THE

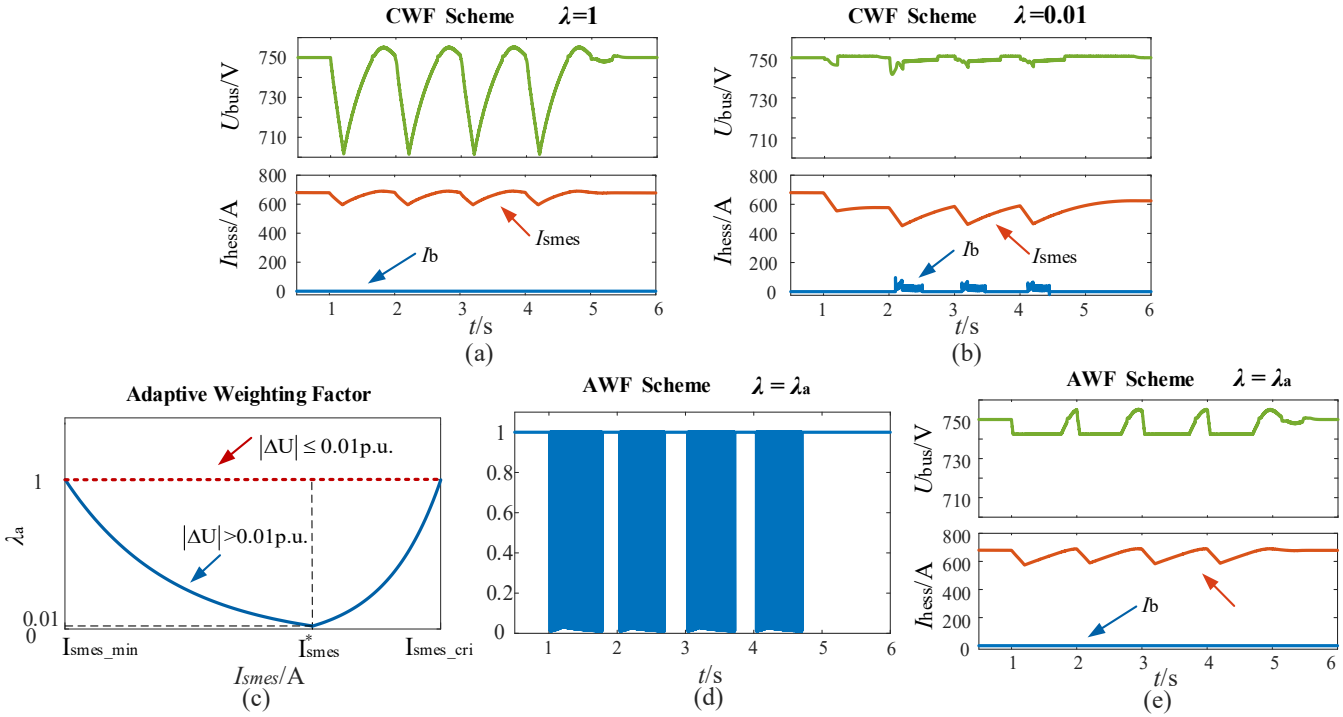

Fig. 3. The response of HESS for different weighting factors. (a) Response of U_{bus} and I_{hess} for λ = 1; (b) Response of U_{bus} and I_{hess} for λ = 0.01; (c) Function of λ_a in relation to SMES current and DC bus voltage tracking error.; (d) behavior of λ_a; (e) Response of U_{bus} and I_{hess} for $\lambda = \lambda_a$;

This article has been accepted for publication in a future issue of this journal, but has not been fully edited. Content may change prior to final publication. Citation information: DOI 10.1109/TTE.2022.3177296, IEEE Transactions on Transportation Electrification

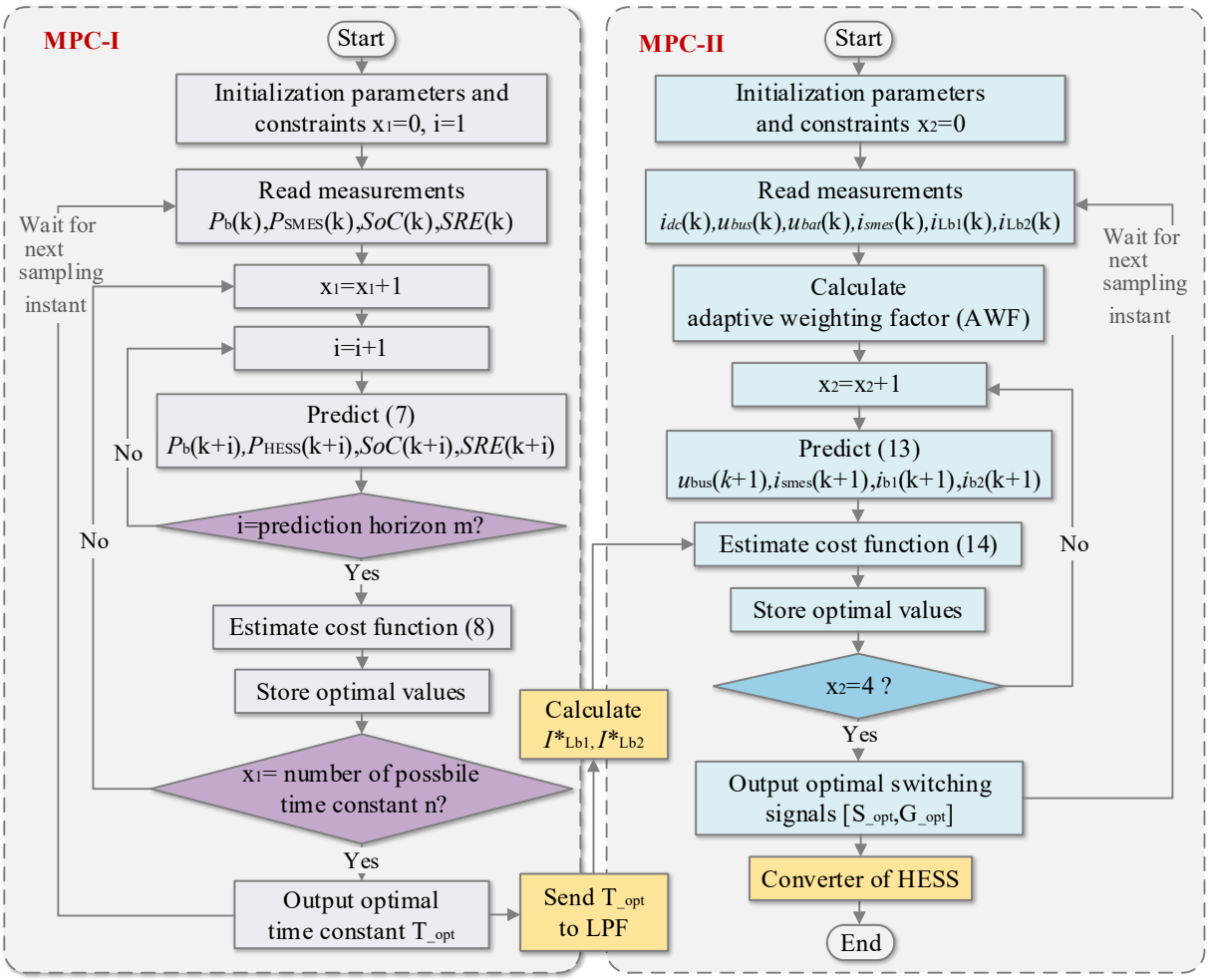

Fig. 4. Flow diagram of the proposed D-MPC control scheme.

MPC-II executes the loop for 4 times to obtain the minimized cost function and the optimal switching state [$S_{\_opt}$, $G_{\_opt}$] that will apply to converters every sampling time.

In general, the MPC-II is related to the result of MPC-I, but MPC-I and MPC-II can run independently using dual core controller. This is because MPC-II can control the charging and discharging of SMES independently only based on the local DC bus signaling. Although the MPC-I based LPF may not output battery power reference immediately due to communication delay, the SMES can also handle the power demands at initial stages until receives the updated battery current reference from the MPC-I. The relatively larger calculation burden and time of MPC-I do not affect the operation of MPC-II.

III. Sizing and Magnet Design

Based on the proposed control scheme, for the two types of pulsed power load (PPL) in naval DC microgrid as mentioned in Section 2.1, battery and SMES should be sized to meet the power and energy requirements. Considering the long-term and short-term power fluctuations in other renewable power generation-based microgrid, some precious works divided the sizing study into two steps [28], [29]: energy dispatching requirements set battery size and power fluctuation mitigating function determines the SMES size. In this work, due to the duration and power value of Type-A PPL (pulsed load) are constant, the sizing of SMES can be determined by the Type-A PPL. The sizing of BESS can be set according to the Type-B PPL (mode change of radar load).

For the BESS, the energy capacity of battery should meet the Type-B PPL load demands. Suppose that the diesel generation system supplies the average power of rated radar load power, and considering the given parameters (Table II in section 4), the battery is sized to be 300 Ah. For the SMES, the power and capacity should be capable of compensating the deficiency power of Type-A PPL during pulse ON, and suppressing the voltage swell during pulse OFF. For the service life extension of battery, the BESS supposed to be standby, and SMES handles the pulsed load independently.

To sum up, the energy and power parameters of SMES should achieve the following objectives:

a) Each pulse energy should be smaller than the normal capacity of the SMES.

b) The rated discharging power of the SMES at pulse ON should be larger than the instantaneous pulsed power.

c) The maximum charging power of the SMES at pulse OFF should be larger than the surplus power.

This article has been accepted for publication in a future issue of this journal, but has not been fully edited. Content may change prior to final publication. Citation information: DOI 10.1109/TTE.2022.3177296, IEEE Transactions on Transportation Electrification

Assuming the power of Type-A PPL is P_{load1}, the duty cycle is D_1, and the frequency of the PPL is T_1 as shown in Fig. 1. The corresponding equations of the objectives above are expressed in (16), (17), and (18) respectively.

$$P_{load1} \cdot T_1 \cdot D_1 = E_{PLL} < E_{SMES\_ref} \quad (16)$$

$$I^*_{smes} \times u^*_{bus} > P_{load1} \quad (17)$$

$$\Delta P_G < I_{smes\_min} \times u^*_{bus} \quad (18)$$

Here, E_{PLL} is the energy consume of one pulse power load and ΔP_G is the increased power of the diesel generator sets during pulse ON, which can be seen as the difference between the rated power P_{G_rated} in normal operating conditions of diesel generator sets and the maximum power limit of them P_{G_max} as given in (19).

$$\Delta P_G = P_{G\_max} - P_{G\_rated} \quad (19)$$

Taken consideration of both conditions of (i) and (iii), the (16) can be modified as:

$$E_{PLL} < E_{SMES\_ref} - E_{SMES\_min} = E_{SMES\_ref} - \frac{1}{2} L_{SC} I^2_{smes\_min} \quad (20)$$

According to (17)-(20), the I^*_{smes} and I_{smes_min} are set to be 680 A and 270 A respectively.

A step-shaped SMES magnet having an inductance of 1.2 H and a critical current of 880 A is used as the reference current of SMES in this paper [31]. It has nine step-shaped pancake assemblies from one end to the other end. The middle assembly (Assembly E) consists of ten serial pancakes, with each pancake wound by fifty coil turns. Its inner and outer radii are 250 mm and 285 mm, respectively.

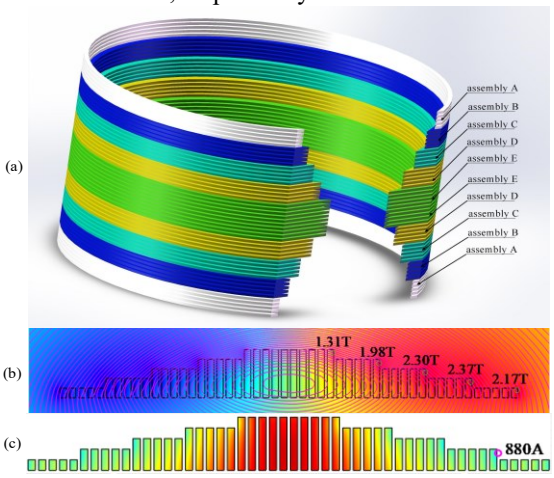

Fig. 5. SMES magnet. (a) Geometric structure profile of the step-shaped SMES magnet; (b) Perpendicular field distribution in the step-shaped scheme; (c) Critical current distribution in the step-shaped scheme.

To construct the step-shaped cross-sectional shape in Fig. 5 and Table I [31], four symmetrical assemblies at two sides are formed by five serial pancakes and named as A, B, C, and D from each coil end to the middle part. Their inner radii are 278 mm, 271 mm, 264 mm, and 257 mm, respectively. When this step-shaped structure scheme is applied, the maximum perpendicular flux density across the superconducting tapes is reduced from about 3.13 T to 2.37 T, and thus the critical current is improved from about 628 A to 880 A accordingly.

TABLE I

SPECIFICATIONS OF THE 1.2-H/880-A STEP-SHAPED MAGNET

Parameter		Value
Structural type		Step-shaped coil
No. of serial pancake assemblies		9
No. of serial pancakes in one assembly		10 (Assembly E) 5 (Assembly A, B, C, and D)
Pancake	Inner radius	250 (Assembly E) 257 (Assembly D) 264 (Assembly C) 271 (Assembly B) 278 (Assembly A)
	Outer radius	285 mm
	Height	4.5 mm

IV. CASE STUDY

The experimental models of shipboard microgrid, which the PPL supplied by DG sets, SMES-battery HESS, have been implemented in StarSim CHIL platform. The batteries, SMES, HESS DC/DC converters, and other main circuits are emulated in MT 6020 Simulator with the time step of 1μs. Controllers in the system are implemented in a MT 1050 RCP (Rapid Control Prototyping) and the sampling frequency is set as 10kHz. The picture of the CHIL platform is given in Fig. 6. Main parameters of the system are listed in Table II. The experimental results of Type-A PPL (laser weapon system) and Type-B PPL (radar load) are illustrated in Fig. 7 and Fig. 8 respectively. The effectiveness of utilizing SMES-battery HESS and the proposed MPC-based control method is shown in the comparison in Fig. 7. While the effectiveness of the proposed D-MPC method is presented by comparison of the traditional constant-time low-pass filtering (CLPF) and the constant weighting factor (CWF) MPC shown in Fig. 8.

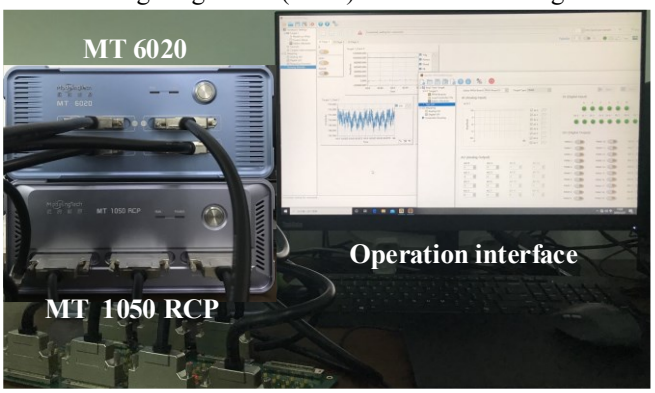

Fig. 6. Hardware platform of HIL experiment.

This article has been accepted for publication in a future issue of this journal, but has not been fully edited. Content may change prior to final publication. Citation information: DOI 10.1109/TTE.2022.3177296, IEEE Transactions on Transportation Electrification

TABLE II

PARAMETERS OF A NAVAL DC MICROGRID

Battery	**Value**	**Load**	**Value**
Rated voltage of battery/V	600	Laser weapon system power/kW	500
Battery capacity /Ah	300	Frequency/Hz	1
Maximum charge current/A	300	Duty cycle	20%
Maximum discharge current/A	450	Rated power of Radar/kW	450
HESS Converters	**Value**	**MPC Controllers**	**Value**
Inductor of battery converter/mH	2	Ts/ms	0.05
Capacitor of HESS/mF	5	Predict horizon of MPC-I/MPC-II	10/1
DC bus voltage/V	750	Control horizon	1
SMES	**Value**	**Diesel generator and its converters**	**Value**
Coil inductance/H	1.2	Rated capacity of synchronous generator/MW	2
Critical current of SMES/A	880	Nominal voltage of synchronous generator /V	400
Rated current of SMES/A	680	Frequency of synchronous generator /Hz	50
Minimum current of SMES/A	270	Capacitor of VSC/mF	50

A. Verifying HESS and MPC

Except PPLs, others load in naval DC microgrids, such as variable speed drives are represented by the resistive load in simulation. At beginning of this case, a 1 MW resistive load is connected in the DC microgrid. In addition, the pulsed load occurs four times in the naval DC microgrid. The HIL experimental results of the power supplied to the load by DG, the batteries, and the SMES as well as the DC bus voltage, the SoC of battery, or state of residual energy (SRE) of SMES under three schemes are shown in Fig. 7 (a) (b) and (c).

Based on PI control without SMES, due to the slow response of the battery, the output power of DG increases rapidly, which will keep over the limit of rectifier of 1.2 MW and results in a destructive effect. Moreover, the batteries discharge every time during pulses ON, and the SoC keep decreasing. This issue results in the negative effect on the battery service lifetime and the over-discharge problem of battery. As for traditional PI control with SMES shown in Fig. 7(b), the SMES has the advantage of fast responses each pulse and is able to absorb energy when pulses off to allow the SRE to recover. The stability of the DC bus voltage is improved. However, even with the introduction of SMES, the number of mode switches for the battery remains at four (from idle mode to discharge mode). As a result, the dynamic response stress of the battery is not improved under the control of LPF because of the saturation effect of the PI loops and low response of PI controller.

Based on the proposed MPC-based method, the SMES is discharging as fast as possible during every pulse ON while the batteries only discharge when the SRE of SMES is not enough to compensate the power demand. And the SRE of SMES recovers as much as possible at every pulse OFF to be ready for dealing with the next pulse. Fig. 7(c) demonstrates that based on the proposed method with SMES, the dynamic performance of DC bus voltage under pulsed load is better and the stability of DC microgrid is improved. In Fig. 7(c), the DC bus voltage is maintained around the reference value with the lowest value of about 738 V (98.4%). While in Fig. 7(a), the lowest value is about 634 V (84.53%), and in Fig. 7(b), the lowest value is 702 V (93.6%).

B. Verifying D-MPC

In this case, three different methods have been conducted to show the superiority of the proposed D-MPC based method during the operation mode change of radar load, which are presented in detail as follows:

Method i: CLPF+CWF: constant low-pass filtering (T=0.16) and constant weighting factor (λ=0.1) based MPC.

Method ii: ALPF+CWF: adaptive low-pass filtering ($T \in [0.01, 0.16]$) and constant weighting factor (λ=0.1) based MPC (MPC-I).

Method iii: ALPF+AWF: adaptive low-pass filtering and adaptive weighting factor ($\lambda_a \in [0.01, 1]$) based MPC (proposed D-MPC).

Fig. 8 shows the experimental results during the Type-B PPL. The radar load power change curve is given in Fig. 8(a).

1) Effectiveness of MPC-I

The effectiveness of the MPC-I based ALPF can be demonstrated by comparing Method i with Method ii in Fig. 8. In the case of CLPF, the DC bus voltage drops more severely with the lowest value of about 670 V (89.33%) as shown in Fig. 8(b) while the DC bus voltage is maintained above 700 V (93.33%) in case of ALPF under Method ii. This is because that at t=2s, the average power of total load increases sharply, the SRE of SMES falls quickly and the battery is required to support the DC bus voltage independently when SRE reaches its minimum limit.

In details, it can be observed from Fig. 8(c) and (d) that the diesel generation system output power is relatively stable (between 1040kW and 1090kW) under all the methods. And based on ALPF, the battery discharge earlier and the output power rising rate is larger than Method i at about t= 2.2 s. This is because that ALPF shares the power between batteries and SMES by considering the SRE of SMES based on MPC-I, Moreover, during t=2.2 s ~2.5 s, the state of residual energy of

This article has been accepted for publication in a future issue of this journal, but has not been fully edited. Content may change prior to final publication. Citation information: DOI 10.1109/TTE.2022.3177296, IEEE Transactions on Transportation Electrification

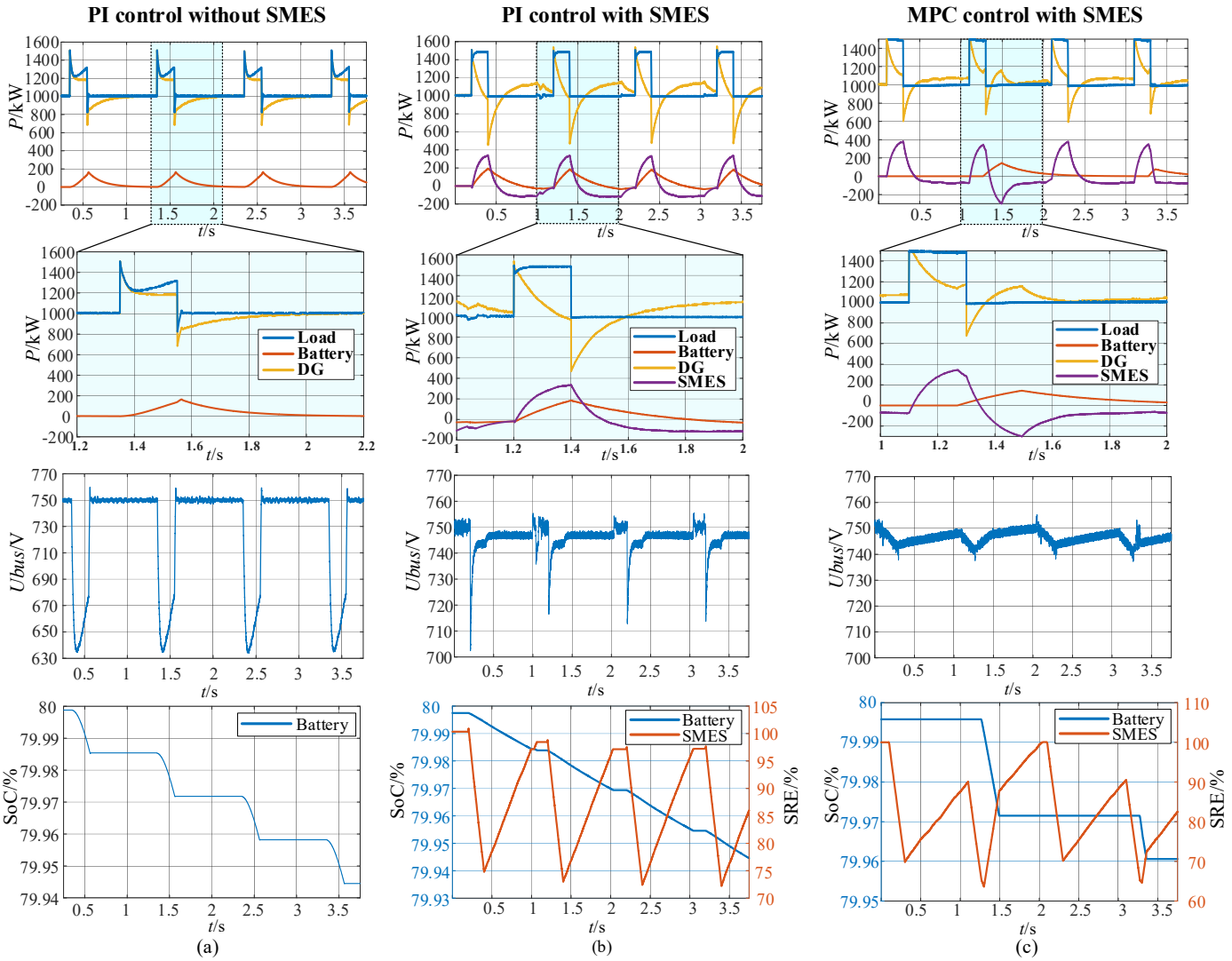

Fig. 7. Comparison among (a) PI control without SMES, (b) PI control with SMES, (c) proposed MPC-based control with SMES under Type-A PPL.

SMES reached its minimum value in Method i and ii as shown in Fig.8(e), and the SMES were out of service. The output power is reduced to zero as shown in Fig. 8(f). Consequently, based on ALPF, the battery can deal with some of the high-frequency unbalanced power by modifying filter time constant; while based on CLPF, the output power of battery is still smooth as shown in Fig. 8(d), thus leads to DC bus voltage drop. The transient power sharing adjustment was implemented by automatic reduction of the filter time constant value by MPC-I

2) Effectiveness of MPC-II

By comparing Method iii with Method i and Method ii, the effectiveness of the proposed AWF MPC-II can be verified. An optimal tradeoff between the objectives of DC bus voltage regulation and energy recovery of SMES was made due to the self-adaptive adjustment of the weighting factor of MPC-II. Fig. 8(b) shows that Methods iii provided stiff DC bus voltage regulation in the presence of PPLs. The DC bus voltage is maintained above 740 V (98.67%).

Under the control of Method iii, Fig. 8(d) shows that the value of battery output power is higher than other methods and responds earlier in order to supply energy to SMES and loads. Thus, the SMES gets a better energy recovery effect, with SRE above 60% as shown in Fig(e). Fig.8(e) and (f) also jointly demonstrate that SMES is able to deal with the high-frequency fluctuation constantly and will not be faced with the problem of SRE reaching the lower limit and then out of service. As a result, the control scheme of ALPF+AWF improves the longevity of the HESS in maintaining the DC bus voltage.

V. CONCLUSION

This article presents a D-MPC control scheme and configuration for a SMES-battery HESS as a buffer to the power demands of pulsed power loads in naval DC microgrid. It aims to regulate the DC bus voltage and manage the power sharing between SMES and battery as well as complying with constraints of several variables. Two cases study of different types of pulsed power loads is carried out in simulation to

This article has been accepted for publication in a future issue of this journal, but has not been fully edited. Content may change prior to final publication. Citation information: DOI 10.1109/TTE.2022.3177296, IEEE Transactions on Transportation Electrification

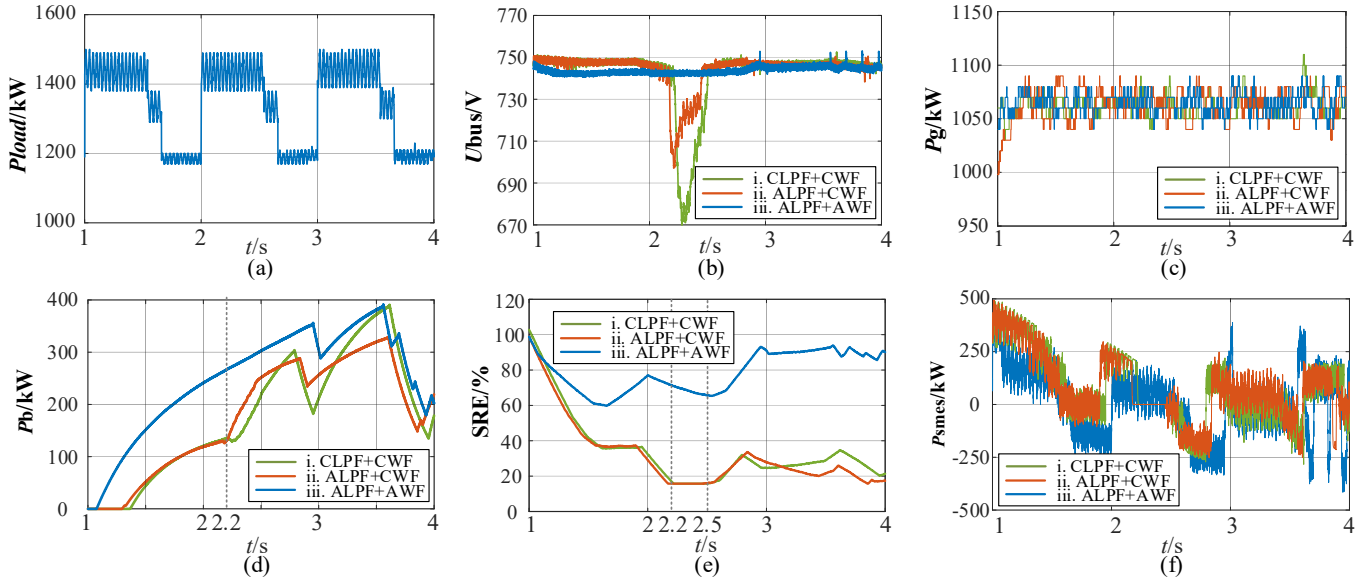

Fig. 8. Simulation results in the presence of Type-B PPL under three different methods. (a) total load power; (b) DC bus voltage; (c) diesel generation system output power; (d) Battery output power; (e) state of residual energy of SMES; (f) SMES output power.

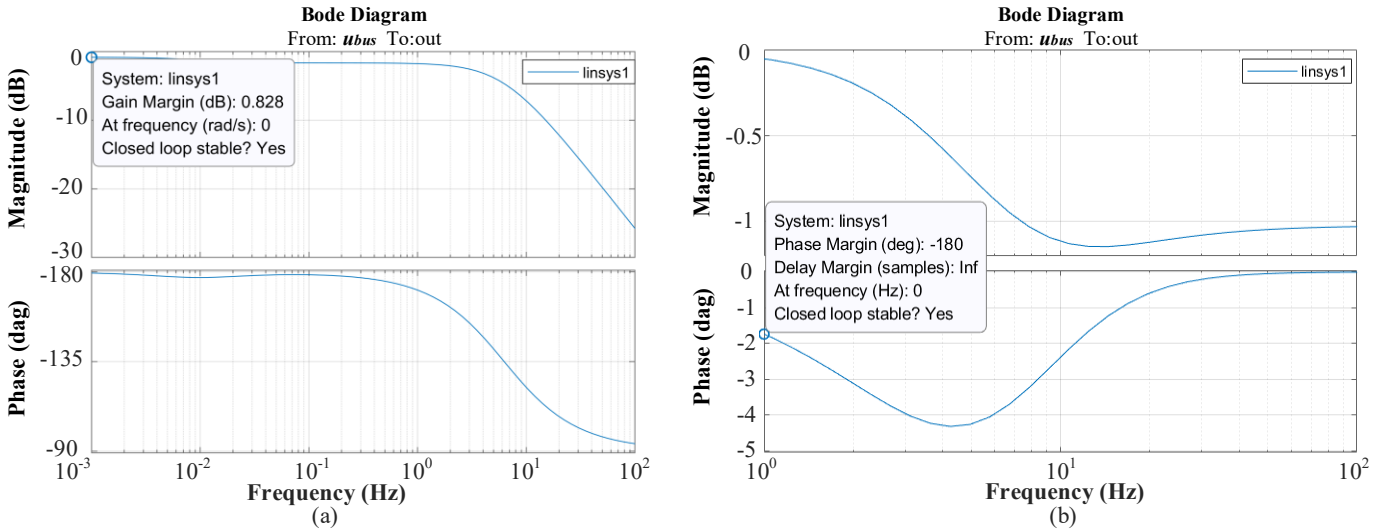

Fig. 9. Bode diagrams for PI control. (a) PI controller for battery; (b)PI controller for SEMS.

verify the benefits of this scheme. Simulation results prove that the HESS incorporating to the DC bus can not only mitigate PPLs effect, but also help to improve the operation stability of the naval DC microgrid. It provides advantages listed as follows.

a) The SMES is directly controlled by the one-step FCS-MPC, which avoids the saturation problem of PI loops and reduces the computational burden to improve the dynamic response time.

b) Low-pass filtering strategy integrates with MPC has adaptive filtering effect to reduce the charge/discharge cycle of battery while avoiding the over-discharge and over-charge problem of HESS.

c) Better DC bus voltage operation stability, as well as better energy recovery performance of SMES, compared with the conventional approaches.

The scheme is also suitable for HESS supplying various plug-and-play loads in high penetration renewable energy power generation systems and likewise has the potential to be applied for other HESS storage systems in aircraft or electric vehicles.

APPENDIX I

Table III shows the parameters of PI controller used in Section IV, A. And Fig. 9 shows the bode diagrams for the PI control. Both Fig.9 (a) and (b) can be exported from MATLAB/Simulink directly.

This article has been accepted for publication in a future issue of this journal, but has not been fully edited. Content may change prior to final publication. Citation information: DOI 10.1109/TTE.2022.3177296, IEEE Transactions on Transportation Electrification

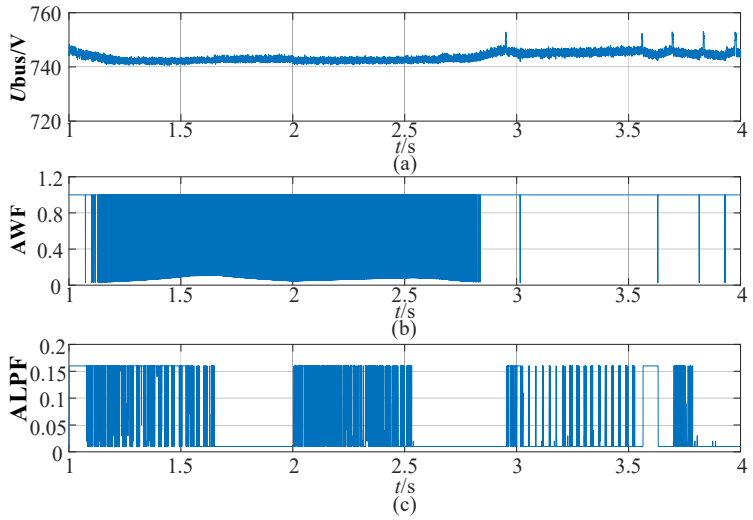

Fig. 10. Changes of AWF and ALPF constants. (a) DC bus voltage; (b) AWF; (c) ALPF.

TABLE III

PARAMETERS OF PI CONTROLLER

Control loop	Parameters	
	Proportionality coefficient	Integral coefficient
Voltage loop of battery	10	0.1
Current loop of battery	10	300
Voltage loop of SMES	4	200
Current loop of SMES	2	100

APPENDIX II

In Fig. 8, a comparison is performed among CLPF+CWF, ALPF+CWF, and ALPF+AWF. The behavior changes of ALPF and AWF constants in time for the presented HIL experiments are shown in Fig. 10.

REFERENCES

[1] Jothibasu, Suma, and S. Santoso, "New electric shipboard topologies for high resiliency," *IEEE Trans. Power Syst*., vol. 33, no. 3, pp. 2975–2983, May 2018.

[2] "IEEE recommended practice for 1 kv to 35 kv medium-voltage DC power systems on ships," *IEEE Std 1709-2018* (Revision of IEEE Std 1709-2010), pp.1-54, Dec. 2018.

[3] A. Maqsood, D. Oslebo, K. Corzine, L. Parsa and Y. Ma, "STFT cluster analysis for DC pulsed load monitoring and fault detection on naval shipboard power systems," *IEEE Trans. Transport. Electrific*., vol. 6, no. 2, pp. 821–831, Jun. 2020.

[4] U. Abhisek, M. Y. Yew, S. Kuntal, "Fault analysis and protection system design for DC grids", *1st ed, Singapore*, SG: Springer, 2020, pp. 1–24.

[5] M. Farhadi and O. A.Mohammed, "Performance enhancement of actively controlled hybrid DC microgrid incorporating pulsed load," *IEEE Trans. Ind. Appl.*, vol. 51, no. 5, pp. 3570–3578, Sep. 2015.

[6] E. Skjong, R. Volden, E. Rødskar, M. Molinas, T. A. Johansen, and J. Cunningham, "Past, present, and future challenges of the marine vessel's electrical power system," *IEEE Trans. Transport. Electrific*., vol. 2, no. 4, pp. 522–537, Dec. 2016.

[7] Z. Xiao, H. Li, H. Fang, et al., "Operation control for improving energy efficiency of shipboard microgrid including bow thrusters and hybrid energy storages," *IEEE Trans. Transport. Electrific*., vol. 6, no. 2, pp. 856–868, Jun. 2020.

[8] M. M. Mardani, M. H. Khooban, A. Masoudian and T. Dragičević, "Model predictive control of DC–DC converters to mitigate the effects of pulsed power loads in naval DC microgrids," *IEEE Trans. Ind. Electron.*, vol. 66, no.7, pp. 5676–5685, Jul. 2019.

[9] X. Lin, R. Zamora, "Controls of hybrid energy storage systems in microgrids: Critical review, case study and future trends," *J Energy Storage*, vol. 47, no. 103884, Mar. 2022.

[10] X. Luo, J. Wang, M. Dooner, et al., "Overview of current development in electrical energy storage technologies and the application potential in power system operation," *Appl. Energy,* vol. 137, pp. 511–536, Jan. 2015.

[11] Z. Nie, X. Xiao, Q. Kang, R. Aggarwal, H. Zhang and W. Yuan, "SMES-battery energy storage system for conditioning outputs from direct drive linear wave energy converters," *IEEE Trans. Appl. Supercond.*, vol. 23, no. 3, pp. 5000705-5000705, Jun. 2013, Art no. 5000705.

[12] J. Hou, Z. Song, H. Park, et al., "Implementation and evaluation of real-time model predictive control for load fluctuations mitigation in all-electric ship propulsion systems," *Appl. Energy*, vol. 230, pp. 62–77, Nov. 2018.

[13] J. Hou, J. Sun, H. Hofmann, "Adaptive model predictive control with propulsion load estimation and prediction for all-electric ship energy management," *Energy,* vol. 150, pp. 877-889, May 2018.

[14] T. Dragicevic, "Model predictive control of power converters for robust and fast operation of ac microgrids," *IEEE Trans. Power Electron.*, vol. 33, no. 7, pp. 6304–6317, Jul. 2018.

[15] Q. Xiao, L. Chen, H. Jia, P. W. Wheeler and T. Dragičević, "Model predictive control for dual active bridge in naval DC microgrids supplying pulsed power loads featuring fast transition and online transformer current minimization," *IEEE Trans. Ind. Electron.,* vol. 67, no. 6, pp. 5197–5203, Jun. 2020.

[16] C. Ju, P. Wang, L. Goel and Y. Xu, "A Two-Layer Energy Management System for Microgrids With Hybrid Energy Storage Considering Degradation Costs," *IEEE Trans. Smart Grid*., vol. 9, no. 6, pp. 6047-6057, Nov. 2018.

[17] P. Lin, T. Zhao, B. Wang, Y. Wang and P. Wang, "A semi-consensus strategy toward multi-functional hybrid energy storage system in DC microgrids," *IEEE Trans. Energy Convers,* vol. 35, no. 1, pp. 336–346, Mar. 2020.

[18] L. Chen, S. Shao, Q. Xiao, L. Tarisciotti, P. W. Wheeler and T. Dragičević, "Model predictive control for dual-active-bridge converters supplying pulsed power loads in naval DC microgrids," *IEEE Trans. Power Electron.,* vol. 35, no. 2, pp. 1957–1966, Feb. 2020.

[19] Y. Shan, J. Hu, K. W. Chan, Q. Fu, and J. M. Guerrero, "Model predictive control of bidirectional DC–DC converters and ac/DC interlinking converters—a new control method for pv-wind-battery

microgrids," *IEEE Trans. Sustain. Energy,* vol. 10, no. 4, pp. 1823–1833, Oct. 2019.

[20] S. Vazquez, J. Rodriguez, M. Rivera, L. G. Franquelo, and M. Norambuena, "Model predictive control for power converters and drives: Advances and trends," *IEEE Trans. Ind. Electron*., vol. 64, no. 2, pp. 935–947, Feb. 2017.

[21] M. M. S. Khan, M. O. Faruque and A. Newaz, "Fuzzy Logic Based Energy Storage Management System for MVDC Power System of All Electric Ship," in *IEEE Trans. Energy Convers.*, vol. 32, no. 2, pp. 798-809, June 2017, doi: 10.1109/TEC.2017.2657327.

[22] H. Shayeghi, F. Monfaredi, A. Dejamkhooy, M. Shafie-khah, J.P.S. Catalão, "Assessing hybrid supercapacitor-battery energy storage for active power management in a wind-diesel system," *Int J Elec Power,* vol. 125, no. 106391 ,2021.

[23] Y. Sun, X. Tang, X. Sun, et al., "Model predictive control and improved low-pass filtering strategies based on wind power fluctuation mitigation," *J. Mod. Power Syst. Clean Energy,* vol. 7, no. 3, pp. 512–524, May 2019.

[24] Y. Bai, H. He, J. Li, S. Li, Y. X. Wang and Q. Yang, "Battery anti-aging control for a plug-in hybrid electric vehicle with a hierarchical optimization energy management strategy," *J. Clean Prod.*, vol. 237, Nov. 2019.

[25] F. Ni, Z. Zheng, Q. Xie, X. Xiao, Y. Zong, C, Huang, "Enhancing resilience of DC microgrids with model predictive control based hybrid energy storage system." *Int J Electr Power Energy Syst* 2021;128:106738.

[26] H. Liao, J. Peng, Y.Wu, et al., "Adaptive Split-Frequency Quantitative Power Allocation for Hybrid Energy Storage Systems," *IEEE Trans. Transport. Electrific,* vol. 7, no. 4, pp. 2306-2317, Dec. 2021.

[27] Q. Sun, D. Xing, H. Alafnan, et al., "Design and test of a new two-stage control scheme for SMES-battery hybrid energy storage systems for microgrid applications," *Appl. Energy,* vol. 253, Nov. 2019.

[28] J. Li, Q. Yang, F. Robinson, et al., "Design and test of a new droop control algorithm for a SMES/battery hybrid energy storage system," *Energy*, vol. 118, pp. 1110–1122, Jan. 2017.

[29] J. Li, A. M. Gee, M. Zhang, et al., "Analysis of battery lifetime extension in a SMES-battery hybrid energy storage system using a novel battery lifetime model," *Energy*, vol.86, pp. 175–185, Jun. 2015.

[30] L. W. Chong, Y. W. Wong, R. K. Rajkumar, D. Isa, "An optimal control strategy for standalone PV system with battery-supercapacitor hybrid energy storage system," *J. Power Sources,* 331, pp. 553–565, Nov. 2016.

[31] X. Y. Chen, and J. X. Jin, "Evaluation of step-shaped solenoidal coils for current-enhanced SMES application," *IEEE Trans. Appl. Supercond.*, vol. 24, no. 5, Oct. 2014, Art. No. 4603404.